Journal of Non-Crystalline Solids 476 (2017) 36–45

Contents lists available at ScienceDirect

Journal of Non-Crystalline Solids

journal homepage: www.elsevier.com/locate/jnoncrysol

Sound insulation properties in low-density, mechanically strong and ductile nanoporous polyurea aerogels

Sadeq Malakooti[a], Habel Gitogo Churu[b], Alison Lee[c], Tingge Xu[a], Huiyang Luo[a], Ning Xiang[d], Chariklia Sotiriou-Leventis[e], Nicholas Leventis[e], Hongbing Lu[a,*]

[a] Department of Mechanical Engineering, The University of Texas at Dallas, Richardson, TX 75080, USA
[b] Department of Mechanical Engineering, LeTourneau University, Longview, TX 75602, USA
[c] AVL Test Systems Inc., Plymouth, MI 48170, USA
[d] Graduate Program in Architectural Acoustics, Rensselaer Polytechnic Institute, Troy, NY 12180, USA
[e] Department of Chemistry, Missouri University of Science and Technology, Rolla, MO 65409, USA

ARTICLE INFO

Keywords:
Polyurea aerogel
Metamaterials
Porous materials
Acoustics
Sound transmission loss
Poroelasticity

ABSTRACT

Aerogels are quasi-stable, nanoporous, low-density, three-dimensional assemblies of nanoparticles. In this paper, an extremely high sound transmission loss for a family of ductile polyurea aerogels (e.g., over 30 dB within 1 to 4 kHz at bulk density 0.25 g/cm^3 and 5 mm thickness) is reported. The fundamental mechanisms behind the aerogel acoustic attenuations are investigated. Sharing striking similarities with acoustic metamaterials, initially, aerogels are studied via a one-dimensional multi degree-of-freedom mass-spring system. Different effects such as spring constant disparity are investigated in regards to the structural vibration wave transmission loss. Results are given for different configurations consistent with the aerogel nano/microstructures. A significant wave attenuation is observed by considering a random spring distribution. In the next step towards modeling such a complex hierarchical and random structural material, the continuum Biot's dynamic theory of poroelasticity is implemented to analyze the experimental sound transmission loss results. In this framework, a two-dimensional plane strain analysis is considered for the interaction of a steady state time-harmonic plane acoustic wave with an infinite aerogel layer immersed in and saturated with air. The effects of bulk density and thickness on the aerogel sound transmission loss are elucidated. By comparing the theoretical results with the experimental observations, this study develops a qualitative/quantitative basis for the dynamics of the aerogel nanoparticle network as well as the air flow and solid vibroacoustic interactions. This basis provides a better understanding on the overall acoustic properties of the aerogels that might also be helpful in the design of the future hierarchical materials.

1. Introduction

For decades if not longer, the quest for light-weight, sound insulating materials has been a central interest of the engineering acoustics community. The challenge primarily originated from the insufficient acoustical performance of the traditional bulky materials,

Abbreviations: PUA, polyurea; pDCPD, polydicyclopentadiene; STL, sound transmission loss; *TL*, transmission loss; DOF, degree of freedom; ω, frequency; n, number of degree of freedoms; X_1 and X_n, the first left and the last right mass displacements; β_1 and β_2, spring constants; $\mathbf{v}$, fluid particle velocity vector; p, acoustic pressure; ∇, gradient operator; c_0, speed of sound in fluid medium; k, acoustic wave number; θ, incident angle; I_R and I_T, reflected and transmitted wave amplitudes; $\tau(\omega,\theta)$, sound transmission coefficient; v_{y1} and v_{y2}, normal fluid velocities in the fluid mediums 1 and 2; p_1 and p_2, acoustic pressures in the fluid mediums 1 and 2; ρ_b, bulk density of the porous material; ρ_s, skeletal density of the porous material; ρ_0, fluid density; ρ_1, bulk density of the solid phase of the porous material; ρ_2, bulk density of the fluid phase of the porous material; h, porosity; σ_{ij}, solid stress components of the porous material; s, mean pore fluid pressure of the porous material; e_{ij}, solid strain components of the porous material; e and ε, solid and fluid volumetric strains of the porous material; $\mathbf{u}$ and $\mathbf{U}$, vector solid and fluid displacement fields of the porous material; N, solid bulk in-vacuo shear modulus of the porous material; E_1, solid bulk in-vacuo Young's modulus of the porous material; η, solid phase loss factor of the porous material; A, Lamé constant of the solid phase of the porous material; υ, in-vacuo Poisson's ratio of the porous material; E_2, fluid bulk modulus of elasticity in the porous material; Q, coupling between fluid and solid phases in the porous material; γ, ratio of fluid specific heats of the porous material; ε', geometrical structure factor of the porous material; σ, steady state macroscopic flow resistivity of the porous material; b, viscous coupling factor of the porous material; ρ_a, inertial coupling parameter of the porous material; $\rho_{11}{}^*$, $\rho_{12}{}^*$ and $\rho_{22}{}^*$, effective complex mass coefficients associated to the viscous energy dissipation in the porous material; C_1 to C_6, unknown coefficients; Kn, Knudsen number; Pr, Prandtl number; λ, mean free path of air molecules; Γ, characteristic length of the porous medium (average pore size diameter); 1D, one dimensional; J_0 and J_1, the first kind Bessel functions of zero and first orders; f_r, fundamental longitudinal resonance frequency; L, panel thickness

* Corresponding author.
E-mail address: hongbing.lu@utdallas.edu (H. Lu).

http://dx.doi.org/10.1016/j.jnoncrysol.2017.09.005
Received 20 June 2017; Received in revised form 22 August 2017; Accepted 1 September 2017
Available online 23 September 2017
0022-3093/

specifically in the low frequency range, which is more important in speech comprehension [1,2]. Empirically, at the low-frequency range, the mean sound transmission loss of a single-layer conventional material increases at an approximately constant rate of 6 dB by doubling the mass per unit area due to the increasing forces of inertia. This phenomenon is referred to as “The Mass Law” [3]. As a result, the current lightweight materials (e.g., acoustical foams) are not able to solely address the realistic engineering demands, and therefore had to be employed in appropriately designed multilayered structures, which are not always an efficient engineering solution due to either thick panels or heavy structures.

In contrast with traditional acoustic materials, aerogels are quasi-stable, low-density 3D assemblies of nanoparticles which are primarily pursued for thermal insulations and often nanoporous hosts of functional guests [4,5]. Aerogels are typically derived from drying wet-gels by turning the pore-filling solvent into a supercritical fluid [5]. Traditional aerogels are mainly based on silica [6]. Interestingly, the experimental and theoretical results on the sound absorbing properties of the silica aerogel structures have revealed a huge improvement compared with their commercial counterparts [7–11]. But, in spite of their very attractive attributes, the application of the silica aerogels has been mostly confined to space exploration due to their structural fragility [5]. The other major limiting factor is the production cost of aerogels, mainly due to the supercritical drying which even limits the size of the final product. To overcome those problems, a new class of aerogels has recently emerged using major polymeric sources, like polyurea.

Polyurea (PUA) aerogels were first reported by De Vos-Biesmans in a 1996 U.S. Patent [12]. Due to the environmental impact concerns, Leventis et al. proposed an alternative synthesis for PUA aerogels by replacing expensive amines with water [13]. Recently, using this approach, we discovered extremely high acoustic attenuation properties in a family of purely organic aerogels, including not only PUA aerogels, but also polydicyclopentadiene (pDCPD) aerogels as well [15]. The acoustic attenuation that was reached was in the 20–40 dB range, in contrast to traditional sound insulation materials, such as polyurethane foam, which can reach up to 5 dB only [15]. Thereby, the main motivation of this work was to study the sound transmission loss (STL) behavior of this family of purely organic aerogels, specifically on PUA aerogels, in pursuit of a better understanding on their main acoustic insulating mechanisms.

In order to make a material with higher sound transmission loss, the sound reflection and/or sound energy absorption should be improved. In the aerogel case, the material is highly porous and therefore the sound energy absorption property is more important to consider as the incident sound pressure wave can penetrate into the material. The sound energy is partly converted into heat within a porous medium via a huge number of internal reflections with the solid network. Meantime, the dimensionless Knudsen number (Kn) can characterize the air flow regime in a porous medium, $Kn = \lambda/\Gamma$, where λ is the mean free path of air molecule (m) and Γ is the characteristic length of the porous medium (m) [16]. The characteristic length can be approximated as the average pore size of the porous material. In most aerogels the average pore size is on the order of 2 to 50 nm, i.e., on the same order of magnitude with the air molecules mean free path [17–19]. In this picture, the Knudsen number becomes close to 1 meaning that both viscous and molecular flows are dominant in the air flow thus facilitating the wave energy dissipation in air saturated aerogel materials. On the other hand, solid-phase sound energy dissipation features can be characterized by their dynamic mechanical properties. Bulk polyurea has been used commercially for more than a decade and is well known as a highly viscoelastic material with strong frequency dependency [20]. Its time dependent properties have been favorably emphasized in different applications, such as blast mitigating coatings [21,22] and acoustic dampening [23].

However, from a different perspective, our aerogels have striking similarities with certain acoustic metamaterials, but their nanostructures are orders of magnitude smaller than those of the latter. Within this framework, the central hypothesis of this work that porous nanostructured materials with multiscale, random, heterogeneous structural elements and porosities would provide highly tortuous paths and synergistic dynamic mechanisms for broadband acoustic attenuation. Using a finite one dimensional (1D) mass-spring model, Jensen has shown that the disparity in spring constants can introduce a phononic band gap in a periodic structure [24]. This is a very promising basis for understanding the physics behind the STL characteristics of aerogels.

In this work, the normal incidence STL of the light-weight eco-friendly synthesized PUA aerogels at different densities are measured and studied using a modified impedance tube technique. In order to study the sound wave propagation in the aerogels, two different modeling perspectives are considered. First, the aerogels are modeled with a conceptual linear monoatomic random mass-spring system in which the identical masses are connected by varying linear elastic springs. Understanding the wave propagation in those 1D structures can shed light on exploring the fundamental mechanisms behind the acoustic attenuation of aerogels. Second, taking advantage of the continuum Biot's dynamic theory of poroelasticity, a quantitative framework on the sound insulating properties of the aerogels is provided to compare them with the experimental normal incidence STL values. The theoretical results and the experimental observations generate a qualitative/quantitative basis for the understanding of the effects of the nanoparticle solid network and its interaction with air flow on the overall acoustic properties of aerogels.

2. Experimental section

2.1. Material synthesis and characterizations

The PUA aerogels of this study were synthesized according to procedures developed and published by the co-authors previously [13]. PUA aerogels at different densities, porosities and morphologies were synthesized by varying the monomer concentration. Bulk densities (ρ_b) were determined from the weight and the physical dimensions of the samples. Skeletal densities (ρ_s) at different bulk density were previously measured and owing to the low variations, here we use the average reported value (1.24 g/cm^3) [13]. Porosities, h, were determined from ρ_b and ρ_s according to $h = 100 \times [(\rho_s - \rho_b)/\rho_s]$. SEM micrographs were obtained from Au-coated samples on a Hitachi model S-4700 field emission microscope.

2.2. Acoustic measurements

The normal incidence STL is the quantity of interest in this research. In order to increase the sensitivity of the standard impedance tube measurement, the three-microphone impedance tube methodology developed by Salissou et al. [25] was implemented here. For geometrically symmetric specimens, as with our aerogel disks, the measurement technique is reduced to three-microphone one-load method with a rigid backing [26], simplifying the measurement and increasing accuracy. Accordingly in this method, referring to Fig. 1a, the test specimen (i.e., material) is mounted at one end of a long, narrow tube, with an acoustic source placed at the opposite end. In addition to two microphones (Mic 1 and 2) in the tube wall upstream, a third microphone (Mic 3) is located in the downstream in a rigid termination directly behind the test sample (see Fig. 1a). The characteristic impedance of the test sample can be determined by measuring the normal-incidence complex reflection coefficient of the material. For more details, one can check [27].

For these measurements, the PUA aerogels are cut in a disk shape (thickness 5 mm and diameter 4 cm) fitted inside the sample holder (a PVC ring, see Fig. 1b). The impedance tube can measure the acoustical properties within a range of frequencies 1 to 4 kHz.

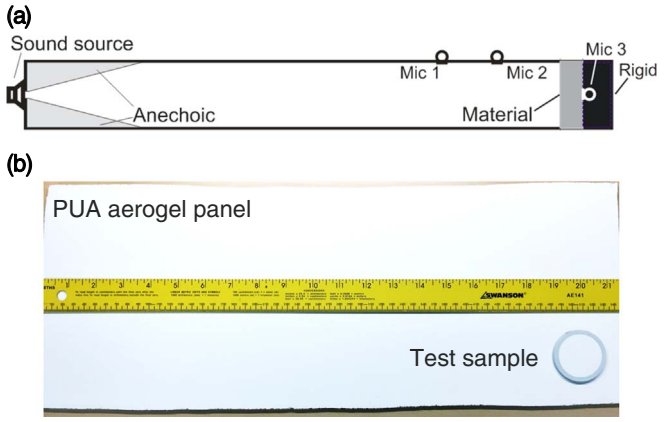

Fig. 1. (a) Schematic of a three-microphone impedance tube for STL measurements; (b) The image of PUA aerogel sample (ρ_b = 0.1 g/cm^3) made in panel form (the test sample cut in a disk shape is shown in the corner).

3. Theoretical modeling

3.1. Random mass-spring model

The structural dynamics of aerogels inherently includes a high level of complexity and randomness due to the aerogel amorphous and hierarchical structure. Fig. 2 shows such a candidate, whereas 2 μm polyurea particles, are connected by a nanofibrous polyurea web, forming a highly random and complex spring-mass system. The random structures can be efficiently abstracted with lower dimensional models with some random structural parameters.

For the sake of simplicity, the aerogels are modeled with a 1D mass-spring system as shown in Fig. 3a [28]. The forced vibration of the system when a time harmonic mechanical force with frequency ω subjected to the left end is analyzed in order to calculate the displacement at the other end mass. The displacement amplitudes can be readily formulated using standard forced vibration analysis. The transmission loss (TL) is then simply introduced as:

$$TL = 20\log_{10}\left(\frac{X_n}{X_1}\right), \tag{1}$$

where X_1 and X_n are the displacements for the first left mass and the last right mass respectively. The number of degree of freedom (DOF) is denoted here by n. In the particular case of a 2-DOF system, the transmission loss can be written as:

$$TL = 20\log_{10}\left(\frac{\beta_1}{\beta_1 + \beta_2 - m\omega^2}\right), \tag{2}$$

where β_1 and β_2 are the spring constants, and m is the mass. Here, a 60-DOF system is considered. The value of the masses are set to 4.02×10^{-14} kg which is the mass of a solid polyurea particle with 2 μm radius. Two situations are taken into account. First, a homogenous system where all the spring constants are set equal to each other (i.e., $\beta = 7.8 \times 10^{-4}$ N/m), and second, a non-homogenous system with a Gaussian random distribution for the spring constants. Fig. 3b and c show the spring constant history of the homogenous and random arrangements. Using the given material properties, the structural vibration transmission loss calculated by Eq. (1) can be analyzed.

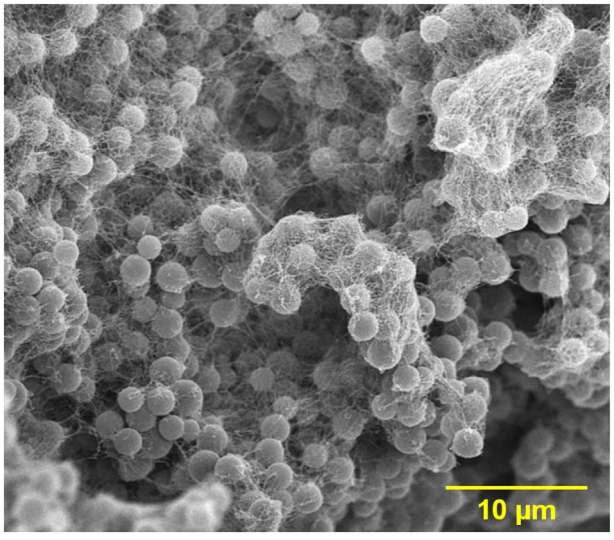

Fig. 2. SEM image of a polyurea aerogel at 0.25 g/cm^3 bulk density [14].

3.2. Wave propagation in poroelastic aerogels

In order to consider the effects of air flow and fluid-solid structural interactions on the wave propagation properties of aerogels, a different approach from discrete mass-spring aerogel model is required. In this research, following the standard techniques of acoustics wave propagation and the Biot's dynamic poroelasticity theory, the wave propagation properties of the porous organic aerogels are modeled and studied. The formulations and the implemented methodology are summarized below.

3.2.1. Acoustic field equations

The Cartesian coordinate system, $\{o;x,y,z\}$, used in this work is shown in Fig. 4. A plate is infinite in the xz-plane and submerged in an unbounded acoustic medium, and the y axis is normal to the plate boundary. An incident time-harmonic plane acoustic wave at an angle θ with respect to the normal of the plate is impinging to the plate.

The field equations for an inviscid ideal compressible fluid medium may be simply expressed in terms of a scalar velocity potential as [3]

$$\mathbf{v} = -\nabla\phi, \tag{3a}$$

$$p = \rho_0\dot{\phi}, \tag{3b}$$

where ρ_0 is the fluid density, $\mathbf{v}$ is the fluid particle velocity vector, p is the acoustic pressure and ∇ is the gradient operator. The scalar velocity potential satisfies the classical wave equation [3],

$$\nabla^2\phi = \frac{1}{c_0^2}\frac{\partial^2\phi}{\partial t^2}, \tag{4}$$

in which c_0 is the speed of sound in fluid medium, and $\nabla^2 = \partial^2/\partial x^2 + \partial^2/\partial y^2$ is the Laplacian. The normalized harmonic solution of Eq. (4) with respect to the incident wave amplitude in the upper and lower fluid mediums may respectively written as [29],

$$\phi_1 = e^{-ik_x x}(e^{-ik_y y} + I_R e^{ik_y y}), \tag{5a}$$

$$\phi_2 = I_T e^{-i(k_x x + k_y y)}, \tag{5b}$$

where $k_x = k\sin\theta$ and $k_y = k\cos\theta$ are the wave numbers in x and y directions, $k = \omega/c_0$ is the acoustic wave number, I_R and I_T are the amplitudes of the reflected and transmitted waves respectively. Here we have assumed harmonic time variations throughout with the $e^{i\omega t}$ dependence suppressed for simplicity.

Using the field equations in Eq. (3), the normal fluid velocity and the acoustic pressure in the upper and lower fluid mediums can be expressed as follows [29]:

$$v_{y1} = -\partial\phi_1/\partial y = -ik_y e^{-ik_x x}(-e^{-ik_y y} + I_R e^{ik_y y}), \tag{6a}$$

$$v_{y2} = -\partial\phi_2/\partial y = ik_y I_T e^{-i(k_x x + k_y y)}, \tag{6b}$$

and

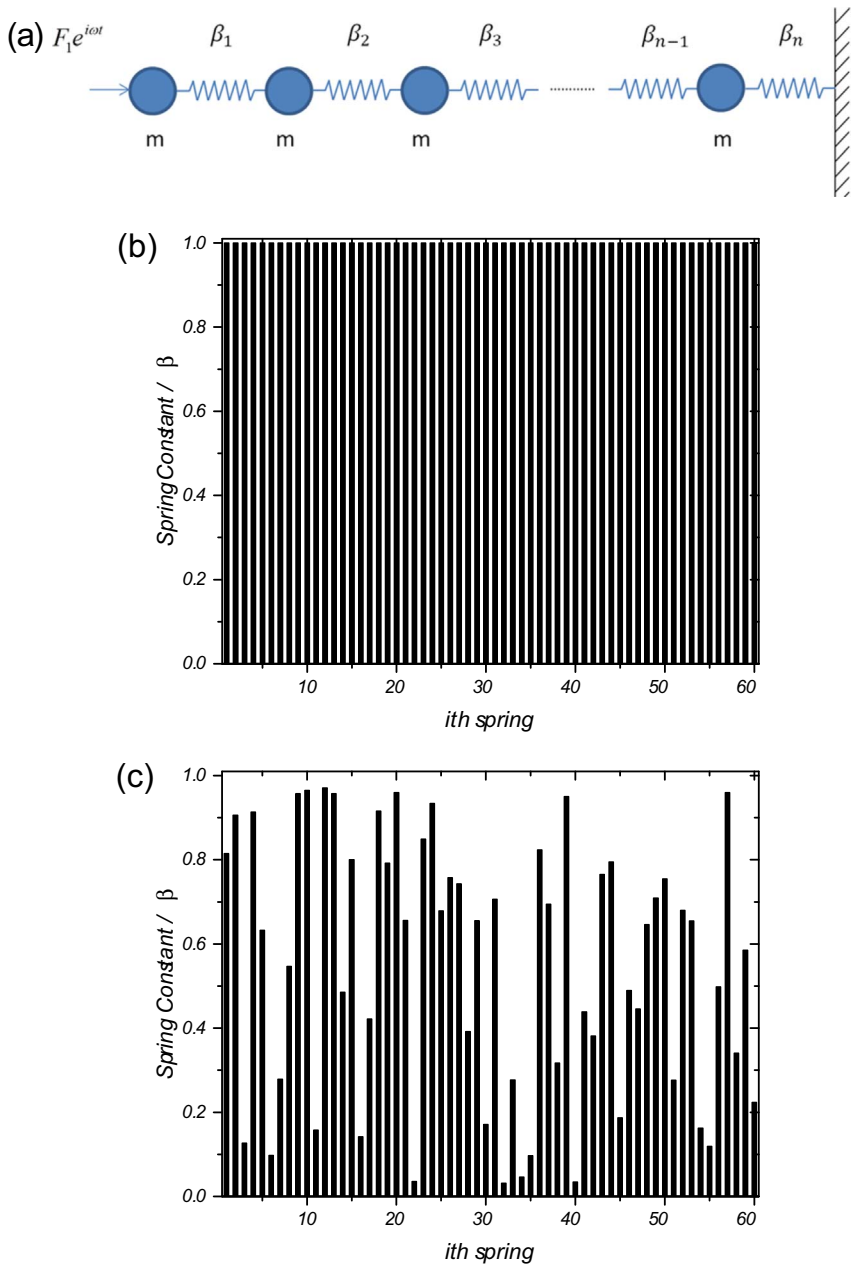

Fig. 3. (a) One dimensional multi-DOF mass-spring system; (b) homogenous and (c) random distributions of the normalized spring constants.

$$p_1 = i\omega\rho_0\phi_1 = i\omega\rho_0 e^{-ik_x x}(e^{-ik_y y} + I_R e^{ik_y y}), \tag{7a}$$

$$p_2 = i\omega\rho_0\phi_2 = i\omega\rho_0 I_T e^{-i(k_x x + k_y y)}, \tag{7b}$$

where v_{y1} and v_{y2} are the normal fluid velocities and p_1 and p_2 are the acoustic pressures in the fluid mediums 1 (upper) and 2 (lower) respectively.

3.2.2. Poroelastic model

The presented theoretical model is based on Biot's dynamic theory of poroelasticity [30,31] which is an efficient two-phase modeling method that can address several important physical properties such as wave speed, attenuation and dispersion. Here the aerogel material is considered as an air-filled porous structure with comparable fluid and solid densities. This theory can formulate the appropriate constitutive equations and equations of motion for the poroelastic media and thus can predict the existence of two types of dilatational (compressional) waves along with one rotational (shear) wave in the coupled fluid-solid network. The theory is summarized below (for more details [30–36]).

The Biot's stress-strain relationship between the fluid and solid strains and applied stress on the solid (σ_{ij}) is written as [32]:

$$\sigma_{ij} = (Ae + Q\varepsilon)\delta_{ij} + 2Ne_{ij}, \tag{8}$$

where $e = \nabla . \mathbf{u}$ and $\varepsilon = \nabla . \mathbf{U}$ are the solid and fluid volumetric strains respectively, $\mathbf{u}$ and $\mathbf{U}$ are the vector solid and fluid displacement fields respectively, $e_{ij} = (u_{i,j} + u_{j,i})/2$, is the solid strain components, $N = E_1/2(1 + \upsilon)$, is the solid bulk in-vacuo shear modulus, E_1 is the solid bulk in-vacuo Young's modulus, υ is the Poisson's ratio, $A = \upsilon E_1/(1 + \upsilon)(1 - 2\upsilon)$, is the Lamé constant of the solid phase, $Q = (1 - h)E_2$, is the coupling between fluid and solid phases, h is material porosity and E_2 is the bulk modulus of elasticity for the fluid in the pores. The mean pore fluid pressure (s) can be also written as [32]:

$$s = R\varepsilon + Qe, \tag{9}$$

where R here is assumed to be hE_2. For air filled cylindrical pores, E_2 can be written in terms of air bulk modulus as [34,35]:

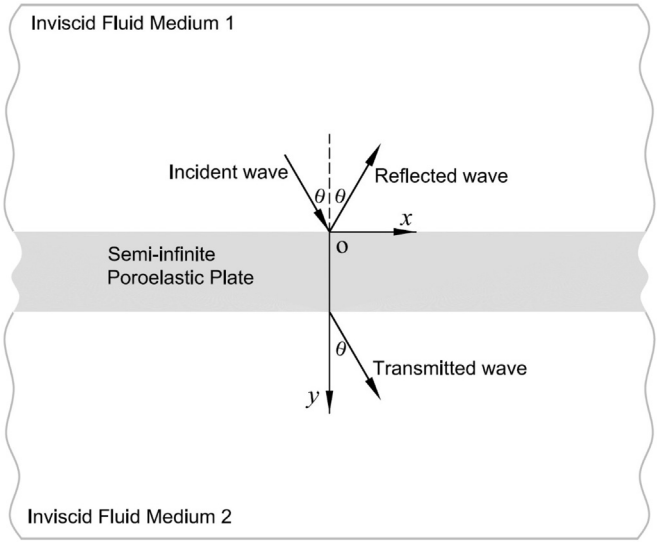

Fig. 4. Two dimensional wave problem geometry of an infinite poroelastic layer in contact with two semi-infinite fluid mediums impinged by plane harmonic acoustic waves.

$$E_2 = E_0\left[1 + \frac{2(\gamma-1)J_1(\mathrm{Pr}^{1/2}\lambda_c\sqrt{-\mathrm{i}})}{\mathrm{Pr}^{1/2}\lambda_c\sqrt{-\mathrm{i}}\,J_0(\mathrm{Pr}^{1/2}\lambda_c\sqrt{-\mathrm{i}})}\right]^{-1}, \tag{10}$$

where $E_0 = \rho_0 {c_0}^2$, γ is the ratio of specific heats, Pr is the Prandtl number, $\lambda_c^2 = \frac{8\omega\rho_0\varepsilon'}{h\sigma}$, J_0 and J_1 are the first kind Bessel functions of zero and first orders respectively. Also ε' is the geometrical structure factor and σ is the steady state macroscopic flow resistivity.

Following the standard methods of continuum mechanics, the equations of motion (linear momentum balance) governing the solid and interstitial fluid displacements under harmonic excitation can be written as [32],

$$N\nabla^2\mathbf{u} + \nabla[(A+N)e + Q\varepsilon] = -\omega^2(\rho_{11}^*\mathbf{u} + \rho_{12}^*\mathbf{U}), \tag{11a}$$

$$\nabla[Qe + R\varepsilon] = -\omega^2(\rho_{12}^*\mathbf{u} + \rho_{22}^*\mathbf{U}), \tag{11b}$$

in which the effective complex mass coefficients (${\rho_{11}}^*$, ${\rho_{12}}^*$ and ${\rho_{22}}^*$) which are associated to the viscous energy dissipation in the porous material due to the relative motion between the phases are written as [32]:

$$\rho_{11}^* = \rho_1 + \rho_a + b/\mathrm{i}\omega, \tag{12a}$$

$$\rho_{12}^* = -\rho_a - b/\mathrm{i}\omega, \tag{12b}$$

$$\rho_{22}^* = \rho_2 + \rho_a + b/\mathrm{i}\omega, \tag{12c}$$

where b is a viscous coupling factor related to the macroscopic flow resistivity of the porous material, ρ_1 and $\rho_2 = h\rho_0$ are the bulk densities of the solid and fluid phases respectively and $\rho_a = \rho_2(\varepsilon' - 1)$ is the inertial coupling parameter between the fluid and solid phases. For cylindrical pores, the coefficient b can be expressed as $b = \mathrm{i}\omega\varepsilon'\rho_2\left(\frac{\rho_c^*}{\rho_0} - 1\right)$ in which ${\rho_c}^*$ can be defined as [34]:

$$\rho_c^* = \rho_0\left[1 - \frac{2J_1(\lambda_c\sqrt{-\mathrm{i}})}{\lambda_c\sqrt{-\mathrm{i}}\,J_0(\lambda_c\sqrt{-\mathrm{i}})}\right]^{-1}. \tag{13}$$

For an isotropic porous material, from the equations of motion, Eq. (11), one can derive a fourth order wave equation for dilatational waves in the solid phase as [36]:

$$\nabla^4 e + A_1\nabla^2 e + A_2 e = 0, \tag{14}$$

where $A_1 = \omega^2({\rho_{11}}^*R - 2{\rho_{12}}^*Q + {\rho_{22}}^*P)/(PR - Q^2)$, $A_2 = \omega^4({\rho_{11}}^*{\rho_{22}}^* - {\rho_{12}}^{*2})/(PR - Q^2)$ and $P = A + 2N$. Eq. (14) has two plane harmonic solutions associated to the two dilatational waves with the wavenumbers given by $k_{1,2}^2 = (A_1 \pm \sqrt{A_1^2 - 4A_2})/2$, [36]. Furthermore the governing wave equation for the rotational wave in the solid can be written as [36]:

$$\nabla^2\boldsymbol{\omega} + k_t^2\boldsymbol{\omega} = 0, \tag{15}$$

where $\boldsymbol{\omega} = \nabla\times\mathbf{u}$ is the solid rotational strain and ${k_t}^2 = (\omega^2/N)/({\rho_{11}}^* - {\rho_{12}}^{*2}/{\rho_{22}}^*)$. The volumetric and rotational strains of the fluid phase can be expressed as [36]:

$$\varepsilon = \nabla.\,\mathbf{U} = \frac{(PR-Q^2)\nabla^2 e + \omega^2(\rho_{11}^*R - \rho_{12}^*Q)e}{\omega^2(\rho_{22}^*Q - \rho_{12}^*R)}, \tag{16a}$$

$$\Omega = \nabla\times\mathbf{U} = -\frac{\rho_{12}^*}{\rho_{22}^*}\boldsymbol{\omega}, \tag{16b}$$

By solving wave equations, Eqs. (14, 15), and subsequently Eq. (16), volumetric and rotational strain fields in fluid and solid phases can be obtained. Boltan et al. have previously showed the plane strain displacement fields for the solid and fluid phases as [36]:

$$u_x = \mathrm{i}k_x\mathrm{e}^{-\mathrm{i}k_x x}\left[\frac{C_1}{k_1^2}\mathrm{e}^{-\mathrm{i}k_{1y}y} + \frac{C_2}{k_1^2}\mathrm{e}^{\mathrm{i}k_{1y}y} + \frac{C_3}{k_2^2}\mathrm{e}^{-\mathrm{i}k_{2y}y} + \frac{C_4}{k_2^2}\mathrm{e}^{\mathrm{i}k_{2y}y}\right] - \mathrm{i}\frac{k_{ty}}{k_t^2}\mathrm{e}^{-\mathrm{i}k_x x}(C_5\mathrm{e}^{-\mathrm{i}k_{ty}y} - C_6\mathrm{e}^{\mathrm{i}k_{ty}y}), \tag{17a}$$

$$u_y = \mathrm{i}\mathrm{e}^{-\mathrm{i}k_x x}\left[\frac{k_{1y}}{k_1^2}C_1\mathrm{e}^{-\mathrm{i}k_{1y}y} - \frac{k_{1y}}{k_1^2}C_2\mathrm{e}^{\mathrm{i}k_{1y}y} + \frac{k_{2y}}{k_2^2}C_3\mathrm{e}^{-\mathrm{i}k_{2y}y} - \frac{k_{2y}}{k_2^2}C_4\mathrm{e}^{\mathrm{i}k_{2y}y}\right] + \mathrm{i}\frac{k_x}{k_t^2}\mathrm{e}^{-\mathrm{i}k_x x}(C_5\mathrm{e}^{-\mathrm{i}k_{ty}y} + C_6\mathrm{e}^{\mathrm{i}k_{ty}y}), \tag{17b}$$

$$U_x = \mathrm{i}k_x\mathrm{e}^{-\mathrm{i}k_x x}\left[b_1\frac{C_1}{k_1^2}\mathrm{e}^{-\mathrm{i}k_{1y}y} + b_1\frac{C_2}{k_1^2}\mathrm{e}^{\mathrm{i}k_{1y}y} + b_2\frac{C_3}{k_2^2}\mathrm{e}^{-\mathrm{i}k_{2y}y} + b_2\frac{C_4}{k_2^2}\mathrm{e}^{\mathrm{i}k_{2y}y}\right] - \mathrm{i}g\frac{k_{ty}}{k_t^2}\mathrm{e}^{-\mathrm{i}k_x x}(C_5\mathrm{e}^{-\mathrm{i}k_{ty}y} - C_6\mathrm{e}^{\mathrm{i}k_{ty}y}), \tag{17c}$$

$$U_y = \mathrm{i}\mathrm{e}^{-\mathrm{i}k_x x}\left[b_1\frac{k_{1y}}{k_1^2}C_1\mathrm{e}^{-\mathrm{i}k_{1y}y} - b_1\frac{k_{1y}}{k_1^2}C_2\mathrm{e}^{\mathrm{i}k_{1y}y} + b_2\frac{k_{2y}}{k_2^2}C_3\mathrm{e}^{-\mathrm{i}k_{2y}y} - b_2\frac{k_{2y}}{k_2^2}C_4\mathrm{e}^{\mathrm{i}k_{2y}y}\right] + \mathrm{i}g\frac{k_x}{k_t^2}\mathrm{e}^{-\mathrm{i}k_x x}(C_5\mathrm{e}^{-\mathrm{i}k_{ty}y} + C_6\mathrm{e}^{\mathrm{i}k_{ty}y}), \tag{17d}$$

where C_1 to C_6 are the unknown coefficients, $b_{1,2} = a_1 - a_2{k_{1,2}}^2$, $a_1 = ({\rho_{11}}^*R - {\rho_{12}}^*Q)/({\rho_{22}}^*Q - {\rho_{12}}^*R)$, $a_2 = (PR - Q^2)/(\omega^2[{\rho_{22}}^*Q - {\rho_{12}}^*R])$, ${k_{1,2y}}^2 = {k_{1,2}}^2 - {k_x}^2$ and $g = -{\rho_{12}}^*/{\rho_{22}}^*$. The stress components in solid and fluid phases can be determined using Eq. (17) substituted into Eqs. (8) and (9) as follows [36].

$$\sigma_y = \mathrm{e}^{-\mathrm{i}k_x x}\left[\left(2N\frac{k_{1y}^2}{k_1^2} + A + b_1Q\right)(C_1\mathrm{e}^{-\mathrm{i}k_{1y}y} + C_2\mathrm{e}^{\mathrm{i}k_{1y}y}) + \left(2N\frac{k_{2y}^2}{k_2^2} + A + b_2Q\right)(C_3\mathrm{e}^{-\mathrm{i}k_{2y}y} + C_4\mathrm{e}^{\mathrm{i}k_{2y}y})\right] + 2N\frac{k_x k_{ty}}{k_t^2}(C_5\mathrm{e}^{-\mathrm{i}k_{ty}y} - C_6\mathrm{e}^{\mathrm{i}k_{ty}y}), \tag{18a}$$

$$\sigma_{xy} = \mathrm{e}^{-\mathrm{i}k_x x}N\left[\frac{2k_x k_{1y}}{k_1^2}(C_1\mathrm{e}^{-\mathrm{i}k_{1y}y} - C_2\mathrm{e}^{\mathrm{i}k_{1y}y}) + \frac{2k_x k_{2y}}{k_2^2}(C_3\mathrm{e}^{-\mathrm{i}k_{2y}y} - C_4\mathrm{e}^{\mathrm{i}k_{2y}y})\right] + \frac{(k_x^2 - k_{ty}^2)}{k_t^2}(C_5\mathrm{e}^{-\mathrm{i}k_{ty}y} + C_6\mathrm{e}^{\mathrm{i}k_{ty}y}), \tag{18b}$$

$$s = e^{-ik_x x}[(Q + b_1 R)(C_1 e^{-ik_{1y} y} + C_2 e^{ik_{1y} y}) + (Q + b_2 R)(C_3 e^{-ik_{2y} y} + C_4 e^{ik_{2y} y})]. \quad (18c)$$

3.2.3. Boundary conditions

The unknown Biot's coefficients are calculated by setting a set of appropriate boundary conditions at the interface of porous layer with the surrounding fluid medium. The specific boundary conditions for this type of interface can be proposed in four conditions:

I. Compatibility of the mean pore fluid pressure (s) with the acoustic pressure (p) in the surrounding fluid:

$$s = -hp, \quad (19)$$

II. Compatibility of the normal stress in the solid phase (σ_y) with the acoustic pressure in the surrounding fluid:

$$\sigma_y = -(1 - h)p, \quad (20)$$

III. Vanishing of the tangential stress component:

$$\sigma_{xy} = 0, \quad (21)$$

IV. Compatibility of the normal volume velocities between the surrounding fluid and the porous material:

$$v_y = i\omega(1 - h)u_y + i\omega h U_y. \quad (22)$$

Eqs. (19) to (22) can be readily written in a matrix form as:

$$[\boldsymbol{M}]_{8\times 8}[\boldsymbol{X}]_{8\times 1} = [\boldsymbol{B}]_{8\times 1}, \quad (23)$$

in which

$$[\boldsymbol{X}]^T = [C_1\ C_2\ C_3\ C_4\ C_5\ C_6\ I_R\ I_T], \quad (24a)$$

$$[\boldsymbol{B}]^T = [-i h\rho_0\omega\ \ i(h-1)\rho_0\omega\ \ ik_y\ \ 0\ \ 0\ \ 0\ \ 0\ \ 0], \quad (24b)$$

where $[\boldsymbol{X}]^T$ and $[\boldsymbol{B}]^T$ are the transpose of $\boldsymbol{X}$ and $\boldsymbol{B}$, respectively. The components of the matrix $\boldsymbol{M}$ are listed in Appendix A. Therefore, by solving the matrix equation, we obtain the reflected (I_R) and transmitted (I_T) sound intensities as a function of incident angle and frequency.

3.2.4. Sound transmission loss

The field quantity of interest in this problem is the sound transmission loss that can be determined as [37]:

$$STL(dB) = 10\log_{10}(1/\tau), \quad (25)$$

where the sound transmission coefficient, $\tau(\omega, \theta) = |I_T|^2/|I_I|^2$, is the ratio of the transmitted to the incident sound intensities. The incident sound intensity in this problem is assumed to be one. In the case of normal incidence STL, the angle is set to zero. This completes the necessary background required for the analysis of the problem.

3.2.5. Material parameterization

For this application, PUA aerogels are considered as air saturated porous materials. The air properties used in this paper are listed in Table 1.

The steady state macroscopic air flow resistivity of the aerogels are estimated using the relation $\sigma = 8\mu/\Gamma^2 h$ [32], where Γ is the average pore size diameter of the aerogel. The change in the average pore size diameter with aerogel bulk densities was found to be negligible and so its average value (Γ = 40.33 nm) is considered in this study [13]. A similar scenario exists for the Poisson's ratio of the aerogels and therefore average Poisson's ratio of 0.22 is used here [13]. However, the bulk Young's modulus significantly changes with bulk density. Experimental studies have shown a power-law relationship ($E_1 = \alpha\rho^{\kappa}$) between aerogel Young's modulus and the aerogel bulk density [38]. Power law fitted parameters, $\alpha$and κ, for our PUA aerogels are obtained as 967.94 m^2/s^2 and 2.004 respectively [13]. In this study, a complex Young's modulus, $E_1(1 + i\eta)$, is considered where η is the solid phase loss factor in order to include the internal friction losses [3]. Typical loss factor at audio frequencies for polyurea ranges from 0.1 to 0.5 [39] and here we used 0.125. The last parameter is the geometrical structure factor of the aerogel (ε'). This value is normally close to 1 for most of the porous materials [32]. All the parameters of the studied aerogels are listed in Table 2.

Table 1
The air properties used in the present calculations.

Density (ρ_0, kg/m^3)	0.909
Speed of sound (c_0, m/s)	328.6
Shear viscosity (μ, Ns/m^2)	1.84×10^{-5}
Prandtl number (Pr)	0.715
Ratio of specific heats (γ)	1.2

Table 2
The aerogel material parameters used in the present calculations.

Bulk density (ρ_b, g/cm^3)	0.11	0.25	0.45
Skeletal density (ρ_s, g/cm^3)	1.24	1.24	1.24
Porosity (h)	0.91	0.80	0.64
Average pore size diameter (Γ, nm)	40.33	40.33	40.33
Static Young's modulus (E_1, MPa)	11.92	61.78	200.62
Average Poisson's ratio (υ)	0.22	0.22	0.22
Loss factor (η)	0.125	0.125	0.125
Air flow resistivity (Ns/m^4)	9.93×10^{10}	1.13×10^{11}	1.42×10^{11}
Geometrical structure factor (ε')	1	1	1

4. Results and discussion

Fig. 5 shows the morphology of the PUA aerogels at different bulk densities. The SEM images reveal that the morphology of the aerogels change from nanofibrous form at low bulk density (0.11 g/cm^3), gradually transitioning to a nano-particulate form in the medium bulk density (0.25 g/cm^3). In that range, nano-fibers evolve into strings of clusters and finally form a predominately nano-particulate pattern at higher bulk densities (0.45 g/cm^3). The structure of pores is highly random in all three samples.

The normal incidence STL measurements of the PUA aerogels at three different bulk densities are shown in Fig. 6. In order to compare the STL values of our aerogels with other relevant materials, we carried out the same experiments on a commercially available aerogel (Spaceloft® Blanket by Aspen Aerogels) consisting of a traditional silica aerogel monolith with embedded glasswool fibers through its bulk, as well as on an acoustic foam (polyurethane based) at similar densities. The STL values of our organic aerogels reached the 20–40 dB range, in contrast to other materials, which can only provide 5 dB or less (see Fig. 6). All acoustical measurements were made in a very high quality condition (i.e., high signal to noise ratio) over the entire frequency range and the repeated experiments on the same material had no significant uncertainty.

As mentioned earlier, in order to find the mechanisms behind this extraordinary sound insulation properties, at the first step, the forced vibration behavior of the aerogels are modeled via a linear mass-spring model. Fig. 7 shows the comparison between the transmission losses as a function of the frequency for the monoatomic configuration when all the spring constants are identical and evenly distributed with the random arrangement, when the spring constants are not identical and randomly distributed (see Fig. 3). This result clearly reveals the idea that in a system with high level of structural randomness, as in our aerogels, there is indeed a super-gap in structural vibration transmission induced by random distribution of the nanoparticles that can eventually lead to a significant reduction in sound transmission loss values. It is worth mentioning that no damping effect was introduced at

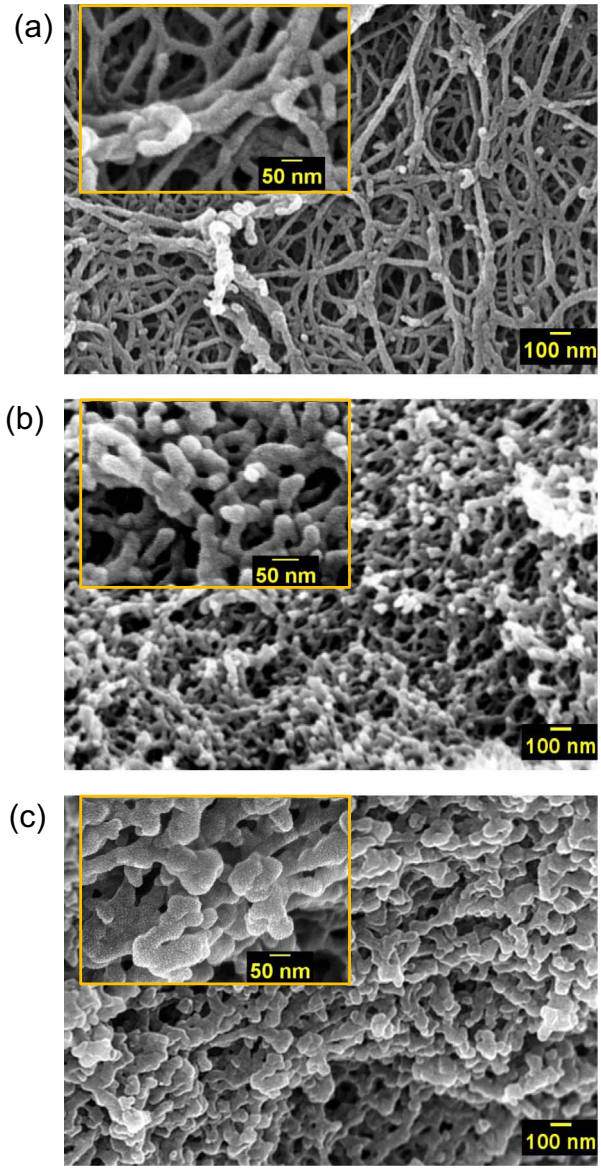

Fig. 5. SEM images of PUA aerogels at different densities: (a) 0.11 g/cm^3, (b) 0.25 g/cm^3 and (c) 0.45 g/cm^3. Higher resolution is given in the subset.

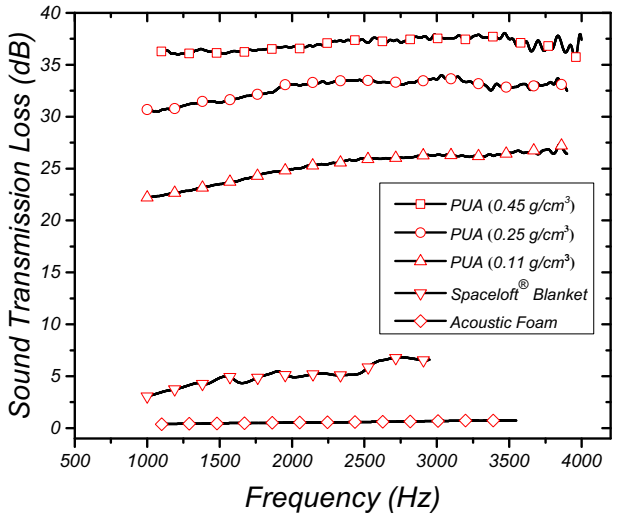

Fig. 6. Experimental STL values of PUA aerogels in comparison with common commercial porous materials.

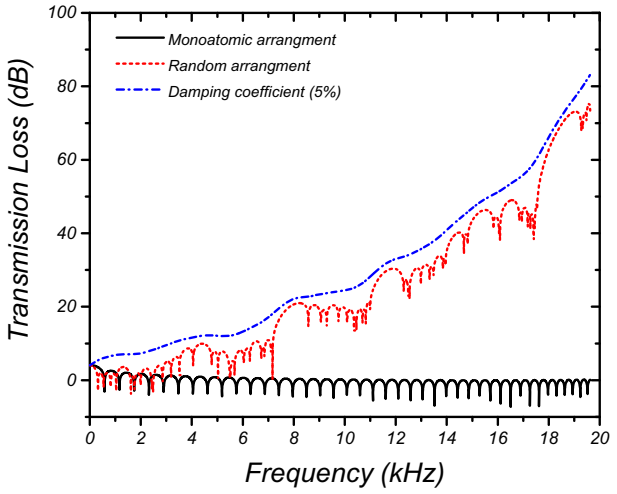

Fig. 7. Vibration transmission loss as a function of frequency for the 60-DOF mass-spring system.

this stage, thereby the super-gap did not originate from any damping energy mechanisms. On the contrary, by introducing viscous damping effects, it was found that the transmission loss resembled the undamped system with slight improvement at low frequencies.

The band-gap that appeared in the random mass-spring system might have originated from the following two wave attenuation mechanisms. First, backscattering might have been introduced by the differences between spring-constants, just as in phononic crystals. Phononic crystals have band gaps because of Bragg scattering due to their periodicity, and acoustic metamaterials due to their local resonant modes. In our 1D model, none of those conditions exist, and thus the random distributed system can be identified as a new potential approach to introducing stop bands. Another reason for the existence of a super-gap is the so-called evanescent wave effect, which generates a wave propagation cut-off frequency above the highest natural frequency [40]. Having a high disparity in spring constants of the random distributed system, the evanescent wave effects induced by the soft springs (smaller spring constants) will dominate and thus attenuate the wave propagation at higher frequencies. For aerogels, the material contains relatively soft springs, and therefore the evanescent wave effects induced by them can be amplified tremendously, especially at high frequencies in high DOF systems, by working synergistically with stop bands (backscattering) effect introduced by the disparity in spring constants. All those mechanistic details render aerogels capable of having a super band-gap for acoustic wave propagations.

Although the mechanisms related to the mass-spring model are very interesting, that model is not predictive in terms of providing a quantitative comparison with actual experimental STL results. In order to rectify that issue, aerogels were considered at face-value, namely as air filled porous materials, and the STL of a thin aerogel layer was calculated using Biot's dynamic theory of poroelasticity.

For three 5-mm thick PUA aerogel disks at different bulk densities, Fig. 8 compares the experimental normal incidence STL values with those predicted by Biot's theory for an infinite aerogel layer in plane strain condition with similar density. Biot's theory, despite all the complexities in the molecular structure of the aerogels, have an overall agreement with the experimental results. This agreement is very good at the high frequency range of the results (2500 Hz and above), while an increasing deviation exists at lower frequencies. For all samples, the average percent error between the experimental results and the theoretical predictions over the entire high frequency range (2500 Hz and above) is about 1% while this error is about 18% at lower frequencies

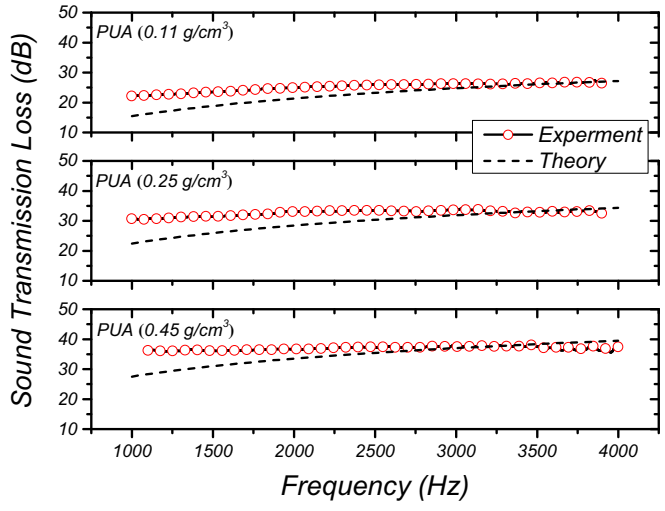

Fig. 8. Experimental and theoretical STL values of PUA aerogels at different densities.

(2500 Hz and below). The reason for that deviation can be attributed to low-frequency airborne sound waves, which are directly related to the air flow properties of the aerogel. Therefore, material parameters such as the flow resistivity, and a structure factor should be calibrated more precisely for that range of frequencies. However, the very good agreement in high frequency region supports sufficiently the applicability of Biot's dynamic theory to the study of sound wave propagation through ductile (i.e., polymeric) aerogels.

In order to illustrate the sensitivity of the STL values to changes in the bulk density of the aerogel, all parameters required by Biot's theory are determined as a function of the bulk density. Fig. 9 shows the contour plot for the normal incidence STL values of a 5-mm thick ductile aerogel infinite plate as a function of bulk density and frequency. It is revealed that the transmission loss gradually increases with aerogel densifying through the whole frequency range. This rate of increase is higher at high frequencies. The variation of STL with the bulk density is very important in the process of the design and manufacturing of potential aerogel-based sound barriers and structures.

Furthermore, the effect of aerogel panel thickness on the normal incidence STL values is studied and the results for the constant bulk

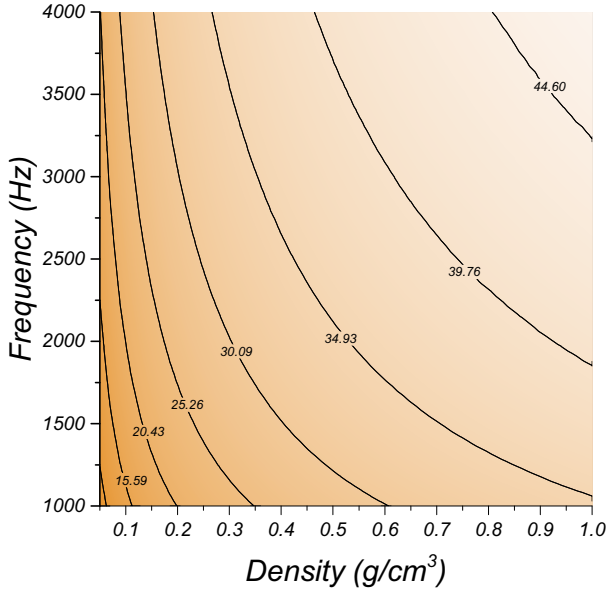

Fig. 9. Contour plot of STL in dB as a function of frequency and bulk density at constant thickness (5 mm).

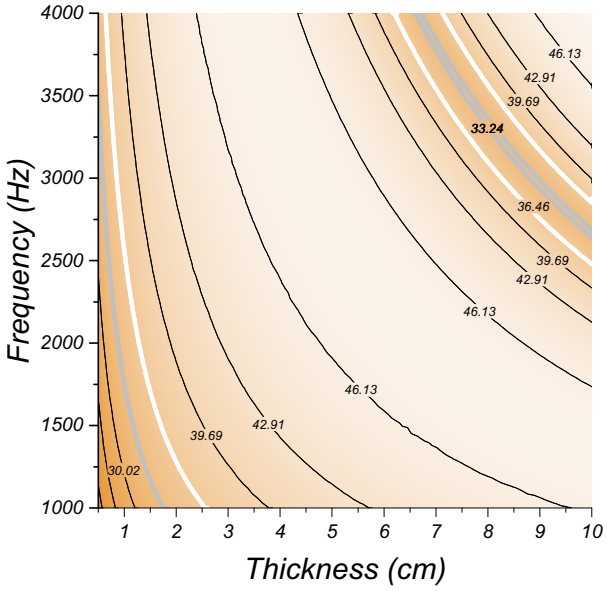

Fig. 10. Contour plot of STL in dB as a function of frequency and thickness at constant bulk density (0.25 g/cm^3).

density of 0.25 g/cm^3 are shown in Fig. 10. The STL values initially increase by thickening the aerogel panel, but later, they are affected by a resonance feature, which leads to decrease STL values. This resonance area is highlighted by white contour lines in Fig. 10.

The nature of that resonance feature can be related to the longitudinal resonance characteristics of the aerogel panel. Considering only the solid phase, the fundamental longitudinal resonance frequency of an infinite porous layer can be approximated as:

$$f_r = \sqrt{\frac{E_1(1-h)}{\rho_s L^2}}, \tag{26}$$

where L is the panel thickness. Eq. (26) can predict the fundamental longitudinal resonance frequency of the aerogel consistent with the results in Fig. 10. For the three different aerogel thicknesses of 7, 8 and 9 cm, Eq. (26) estimates the fundamental longitudinal resonance frequencies to be 3175.93 Hz, 2778.94 Hz and 2470.17 Hz, respectively.

5. Conclusion

In this paper, we have reported an extraordinary sound transmission loss for a family of polyurea aerogels. The goal of this work was to present some preliminary analytical models on the porous aerogel materials with nanoscale morphologies, in order to help us understand their significant acoustical behavior. Using a one dimensional mass-spring system with a random spring constant distribution, the aerogel random and amorphous structure was modeled. The vibration transmission loss results revealed a broadband vibration gap feature for such systems originated mainly from their structural randomness. This simple model clearly indicates that a nanostructured random and amorphous material (i.e., aerogels) can act as a wave transmission attenuator for a certain frequency range. Then, the acoustic wave propagation in aerogels was modeled based on the Biot's theory of dynamic poroelasticity. The theoretical normal incidence sound transmission loss values were compared with the experimental results at different aerogel bulk densities. An overall good agreement was obtained for all densities, which supports the feasibility of the Biot's theory based implementation on the aerogel wave propagation modeling applications. The effects of bulk density and panel thickness on the sound transmission loss behavior were studied. Some longitudinal resonance features were obtained in the sound transmission loss results of the aerogel panels.

Lastly, we should mention that there is still a need to establish a

direct connection between the true micro/nanostructure of each synthesized aerogel sample with the theoretical model. The presented models and methodologies are only able to model a general picture of this complex and hierarchical problem. Despite of the acceptable Biot's performance, for instance, the low frequency deviation between the theory and the experiment needs to be fully understood. Either more detailed and accurate Biot's based material characterizations or generating micro and nanoscale simulation results based on MD or first-principle based models can expand our understanding and lead us to a better and more clear picture of the wave propagation properties of aerogels.

Acknowledgments

The support by AFOSR FA9550-14-1-0227, NSF CMMI-1636306, CMMI-1661246, and ECCS-1307997, and Nashi New Materials, Inc. China is acknowledged. N. L. and C. S. -L. thank the Army Research Office for financial support under Award Number W911NF-14-1-0369, and Covestro LLC (formerly Bayer Corporation U.S.A.) for the generous supply of Desmodur N3300A. H. L. also thanks the Luis A. Beecherl Jr. Chair for additional support.

Appendix A

The nonzero elements of $[\boldsymbol{M}]$ are listed below.

$$M_{11} = Q + b_1R,$$
$$M_{12} = Q + b_1R,$$
$$M_{13} = Q + b_2R,$$
$$M_{14} = Q + b_2R,$$
$$M_{17} = \mathrm{i}h\rho_0\omega,$$
$$M_{21} = A + 2N\frac{k_{1y}^2}{k_1^2} + b_1Q,$$
$$M_{22} = A + 2N\frac{k_{1y}^2}{k_1^2} + b_1Q,$$
$$M_{23} = A + 2N\frac{k_{2y}^2}{k_2^2} + b_2Q,$$
$$M_{24} = A + 2N\frac{k_{2y}^2}{k_2^2} + b_2Q,$$
$$M_{25} = 2N\frac{k_{ty}k_x}{k_t^2},$$
$$M_{26} = -2N\frac{k_{ty}k_x}{k_t^2},$$
$$M_{27} = \mathrm{i}\omega\rho_0(1-h),$$
$$M_{31} = \omega\frac{k_{1y}}{k_1^2}[(1-b_1)h-1],$$
$$M_{32} = -\omega\frac{k_{1y}}{k_1^2}[(1-b_1)h-1],$$
$$M_{33} = \omega\frac{k_{2y}}{k_2^2}[(1-b_2)h-1],$$
$$M_{34} = -\omega\frac{k_{2y}}{k_2^2}[(1-b_2)h-1],$$
$$M_{35} = \omega\frac{k_x}{k_t^2}[(1-g)h-1],$$
$$M_{36} = \omega\frac{k_x}{k_t^2}[(1-g)h-1],$$
$$M_{37} = \mathrm{i}k_y,$$
$$M_{41} = 2N\frac{k_{1y}k_x}{k_1^2},$$
$$M_{42} = -2N\frac{k_{1y}k_x}{k_1^2},$$
$$M_{43} = 2N\frac{k_{2y}k_x}{k_2^2},$$
$$M_{44} = -2N\frac{k_{2y}k_x}{k_2^2},$$
$$M_{45} = N\frac{(k_x^2-k_{ty}^2)}{k_t^2},$$
$$M_{46} = N\frac{(k_x^2-k_{ty}^2)}{k_t^2},$$
$$M_{51} = \mathrm{e}^{-\mathrm{i}k_{1y}}L(Q+b_1R),$$
$$M_{52} = \mathrm{e}^{\mathrm{i}k_{1y}}L(Q+b_1R),$$
$$M_{53} = \mathrm{e}^{-\mathrm{i}k_{2y}}L(Q+b_2R),$$
$$M_{54} = \mathrm{e}^{\mathrm{i}k_{2y}}L(Q+b_2R),$$
$$M_{58} = \mathrm{i}h\rho_0\omega\mathrm{e}^{-\mathrm{i}k_y}L,$$
$$M_{61} = \mathrm{e}^{-\mathrm{i}k_{1y}L}\left(A + b_1Q + 2N\frac{k_{1y}^2}{k_1^2}\right),$$
$$M_{62} = \mathrm{e}^{\mathrm{i}k_{1y}L}\left(A + b_1Q + 2N\frac{k_{1y}^2}{k_1^2}\right),$$
$$M_{63} = \mathrm{e}^{-\mathrm{i}k_{2y}L}\left(A + b_2Q + 2N\frac{k_{2y}^2}{k_2^2}\right),$$
$$M_{64} = \mathrm{e}^{\mathrm{i}k_{2y}L}\left(A + b_2Q + 2N\frac{k_{2y}^2}{k_2^2}\right),$$
$$M_{65} = \mathrm{e}^{-\mathrm{i}k_{ty}L}\left(2N\frac{k_{ty}k_x}{k_t^2}\right),$$
$$M_{66} = -\mathrm{e}^{\mathrm{i}k_{ty}L}\left(2N\frac{k_{ty}k_x}{k_t^2}\right),$$
$$M_{68} = -\mathrm{i}\mathrm{e}^{-\mathrm{i}k_y}L(h-1)\rho_0\omega,$$
$$M_{71} = \mathrm{e}^{-\mathrm{i}k_{1y}L}\omega\frac{k_{1y}}{k_1^2}[(1-b_1)h-1],$$
$$M_{72} = -\mathrm{e}^{\mathrm{i}k_{1y}L}\omega\frac{k_{1y}}{k_1^2}[(1-b_1)h-1],$$
$$M_{73} = \mathrm{e}^{-\mathrm{i}k_{2y}L}\omega\frac{k_{2y}}{k_2^2}[(1-b_2)h-1],$$
$$M_{74} = -\mathrm{e}^{\mathrm{i}k_{2y}L}\omega\frac{k_{2y}}{k_2^2}[(1-b_2)h-1],$$
$$M_{75} = \mathrm{e}^{-\mathrm{i}k_{ty}L}\omega\frac{k_x}{k_t^2}[(1-g)h-1],$$
$$M_{76} = \mathrm{e}^{\mathrm{i}k_{ty}L}\omega\frac{k_x}{k_t^2}[(1-g)h-1],$$
$$M_{78} = -\mathrm{i}\mathrm{e}^{-\mathrm{i}k_y}Lk_y,$$
$$M_{81} = \mathrm{e}^{-\mathrm{i}k_{1y}L}\left(2N\frac{k_{1y}k_x}{k_1^2}\right),$$
$$M_{82} = -\mathrm{e}^{\mathrm{i}k_{1y}L}\left(2N\frac{k_{1y}k_x}{k_1^2}\right),$$
$$M_{83} = \mathrm{e}^{-\mathrm{i}k_{2y}L}\left(2N\frac{k_{2y}k_x}{k_2^2}\right),$$
$$M_{84} = -\mathrm{e}^{\mathrm{i}k_{2y}L}\left(2N\frac{k_{2y}k_x}{k_2^2}\right),$$
$$M_{85} = \mathrm{e}^{-\mathrm{i}k_{ty}L}N\left(\frac{k_x^2-k_{ty}^2}{k_t^2}\right),$$
$$M_{86} = \mathrm{e}^{\mathrm{i}k_{ty}L}N\left(\frac{k_x^2-k_{ty}^2}{k_t^2}\right).$$

References

[1] L.L. Beranek, I.L. Ver, Noise and Vibration Control Engineering: Principles and Applications, John Wiley & Sons, 1992.
[2] D.A. Bies, C.H. Hansen, Engineering Noise Control: Theory and Practice, 4th edition, Spon Press, 2009.
[3] A.D. Pierce, Acoustics: An Introduction to Its Physical Principles and Applications, Acoustical Society of America, 1989.
[4] A.C. Pierre, G.M. Pajonk, Chemistry of aerogels and their applications, Chem. Rev. 102 (2002) 4243–4266.
[5] M.A. Aegerter, N. Leventis, M. Koebel, Aerogels Handbook: Advances in Sol–Gel

Derived Materials and Technologies, Springer, 2011.
[6] H. Maleki, L. Durães, A. Portugal, An overview on silica aerogels synthesis and different mechanical reinforcing strategies, J. Non-Cryst. Solids 385 (2014) 55–74.
[7] L. Forest, V. Gibiat, T. Woignier, Biot's theory of acoustic propagation in porous media applied to aerogels and alcogels, J. Non-Cryst. Solids 225 (1998) 287–292.
[8] V. Gibiat, O. Lefeuvre, T. Woignier, J. Pelous, J. Phalippou, Acoustic properties and potential applications of silica aerogels, J. Non-Cryst. Solids 186 (1995) 244–255.
[9] S. Caponi, A. Fontana, M. Montagna, O. Pill, F. Rossi, F. Terki, T. Woignier, Acoustic attenuation in silica porous systems, J. Non-Cryst. Solids 322 (2003) 29–34.
[10] J.P. Arenas, M.J. Crocker, Recent trends in porous sound-absorbing materials, J. Sound Vib. 44 (2010) 12–18.
[11] P. Yan, B. Zhou, A. Du, Synthesis of polyimide cross-linked silica aerogels with good acoustic performance, RSC Adv. 4 (2014) 58252–58259.
[12] R. De Vos and G. L. J. G. Biesmans, Organic aerogels, U.S. Patent 5,484,818 (16 January 1996).
[13] N. Leventis, C. Sotiriou-Leventis, N. Chandrasekaran, S. Mulik, Z.J. Larimore, H. Lu, G. Churu, J.T. Mang, Multifunctional polyurea aerogels from isocyanates and water. A structure–property case study, Chem. Mater. 22 (2010) 6692–6710.
[14] N. Leventis, C. Chidambareswarapattar, A. Bang, C. Sotiriou-Leventis, Cocoon-in-web-like superhydrophobic aerogels from hydrophilic polyurea and use in environmental remediation, ACS Appl. Mater. Interfaces 6 (2014) 6872–6882.
[15] H. Lu, N. Xiang, N. Leventis and C. Sotiriou-Leventis, Acoustic attenuators based on porous nanostructured materials, U.S. Patent 9,068,346 (30 June 2015).
[16] S.Q. Zeng, A. Hunt, R. Greif, Transport properties of gas in silica aerogel, J. Non-Cryst. Solids 186 (1995) 264–270.
[17] C. Stumpf, K.V. Gassler, G. Reichenauer, J. Fricke, Dynamic gas flow measurements on aerogels, J. Non-Cryst. Solids 145 (1992) 180–184.
[18] N. Husing, U. Schubert, Aerogels-airy materials: chemistry, structure, and properties, Angew. Chem. Int. Ed. 37 (1998) 22–45.
[19] D.A. Tayurskii, K. Matsumoto, On the sound propagation in silica aerogels filled in by normal and supercritical helium, Magn. Reson. Solids 1 (2004) 213–220.
[20] C.M. Roland, J.N. Twigg, Y. Vu, P.H. Mott, High strain rate mechanical behavior of polyurea, Polymer 48 (2007) 574–578.
[21] J.S. Davidson, J.R. Porter, R.J. Dinan, M.I. Hammons, J.D. Connell, Explosive testing of polymer retrofit masonry walls, J. Perform. Constr. Facil. 18 (2004) 100–106.
[22] C. Roland, Rubber Technologist's Handbook, vol. 2, Rapra, 2007.
[23] R.D. Corsaro, L.H. Sperling, Sound and Vibration Damping with Polymers, American Chemical Society, 1990.
[24] J.S. Jensen, Phononic band gaps and vibrations in one-and two-dimensional mass–spring structure, J. Sound Vib. 266 (2003) 1053–1078.
[25] Y. Salissou, R. Panneton, O. Doutres, Complement to standard method for measuring normal incidence sound transmission loss with three microphones, J. Acoust. Soc. Am. 131 (2012) EL216–EL222.
[26] Y. Salissou, R. Panneton, Wideband characterization of the complex wave number and characteristic impedance of sound absorbers, J. Acoust. Soc. Am. 128 (2010) 2868–2876.
[27] C. Fackler, N. Xiang, G. Churu, D.P. Mohite, N. Leventis, C. Sotiriou-Leventis, H. Lu, Experimental investigation of the acoustic attenuation by monolithic polyurea aerogels, Proceeding of 41st International Congress and Exposition on Noise Control Engineering, New York, USA, 19–22 August 2012, pp. 2678–2682.
[28] G. Churu, T. Xu, N. Xiang, N. Leventis, H. Lu, Acoustic attenuation in aerogels, Proceeding of the 9th International Conference on the Mechanics of Time Dependent Materials, Montreal, Canada, 27–30 May 2014, pp. 65–66.
[29] S. Malakooti, N. Mohammadi, M.J. Mahjoob, K. Mohammadi, Identification of adhesive bond in a multi-layered structure via sound insulation characteristics, J. Mech. 26 (2010) 363–372.
[30] M.A. Biot, Theory of propagation of elastic waves in a fluid-saturated porous solid I. Low-frequency range. II. Higher frequency range, J. Acoust. Soc. Am. 28 (1956) 168–191.
[31] M.A. Biot, Mechanics of deformation and acoustic propagation in porous media, J. Appl. Phys. 33 (1962) 1482–1498.
[32] J.F. Allard, N. Atalla, Propagation of Sound in Porous Media: Modelling Sound Absorbing Materials, 2nd edition, John Wiley & Sons, 2009.
[33] J. Zhou, A. Bhaskar, X. Zhang, Sound transmission through a double panel construction lined with poroelastic material in the presence of mean flow, J. Sound Vib. 332 (2013) 3724–3734.
[34] K. Attenborough, Acoustical characteristics of porous materials, Phys. Rep. 82 (1982) 179–227.
[35] C. Zwikker, C.W. Kosten, Sound Absorbing Materials, Elsevier, 1949.
[36] J.S. Bolton, N.-M. Shiau, Y.J. Kang, Sound transmission through multi-panel structures lined with elastic porous materials, J. Sound Vib. 191 (1996) 317–347.
[37] F. Fahy, Foundations of Engineering Acoustics, Academic Press, 2001.
[38] H. Fan, C. Hartshorn, T. Buchheit, D. Tallant, R. Assink, R. Simpson, D.J. Kissel, D.J. Lacks, S. Torquato, C.J. Brinker, Modulus–density scaling behavior and framework architecture of nanoporous self-assembled silicas, Nat. Mater. 6 (2007) 418–423.
[39] J. Qiao, A.V. Amirkhizi, K. Schaaf, S. Nemat-Nasser, G. Wu, Dynamic mechanical and ultrasonic properties of polyurea, Mech. Mater. 43 (2011) 598–607.
[40] P.A. Deymier, Acoustic Metamaterials and Phononic Crystals, Springer, 2013.